Int. J. Heat Mass Transfer. Vol. 32, No. 8, pp. 1491–1499, 1989
Printed in Great Britain

0017-9310/89 $3.00 + 0.00

Turbulent heat transfer in rectangular ducts with repeated-baffle blockages

M. MOLKI and A. R. MOSTOUFIZADEH
Department of Mechanical Engineering, Esfahan University of Technology, Esfahan, Iran

(*Received* 25 *April* 1988 *and in final form* 6 *December* 1988)

Abstract—An experimental study is conducted to investigate heat transfer and pressure drop in a rectangular duct with repeated-baffle blockages. The baffles are arranged in a staggered fashion with fixed axial spacing. The transfer coefficients are evaluated in the periodic fully developed and entrance regions of the duct. The presence of the baffles enhances these coefficients. The entrance length of the duct is substantially reduced by the baffles. Finally, pressure drop and heat transfer data are employed to evaluate the thermal performance of the duct.

INTRODUCTION

FORCED CONVECTION heat transfer in straight smooth ducts has been the subject of study in many experimental and theoretical investigations, and a large amount of useful information is available in the literature. However, the special cases such as the effect of surface roughness [1, 2], wall corrugations [3], baffle blockages [4], and other geometric factors on heat transfer characteristics of turbulent duct flows have received relatively less attention. The present investigation is concerned with one of these special cases, namely, the effect of repeated-baffle blockages on convective heat transfer in rectangular ducts.

There are many practical situations where baffles are employed to enhance heat transfer. One familiar example is the shell-and-tube heat exchanger. The thermal resistance is usually larger on the shell side, and the baffles are deployed along the tube bundle in order to guide and direct the fluid to move perpendicular to the tubes and thus to increase the shell-side heat transfer coefficient. Also, the baffles (fins) might be attached to the walls of the flow passages to provide additional surface area for heat transfer and to promote turbulence. Another example is in cooling the modern multipass turbine blades. It should be noted that heat transfer enhancement in turbine blades is usually accomplished by installing turbulence promoters such as artificial roughness [5]. As an alternative, one may employ baffle blockages to promote turbulence and to cause improved mixing by installing the baffles in a staggered manner in the internal flow passages of the turbine blades.

In the present investigation, the conventional direct method of resistance (Ohmic) heating was replaced by a more accurate mass transfer method known as the naphthalene sublimation technique. This technique not only eliminated the extraneous thermal losses which usually exist in heat transfer experiments, but it also enabled us to have a better control over the boundary conditions and to establish a well-defined boundary condition at the walls of the duct. The mass transfer results obtained by this technique can subsequently be converted to the heat transfer results via the well-known analogy between the heat and mass transfer processes. The theoretical basis for the analogy is discussed by Eckert [6]. In this regard the terms heat and mass transfer are used interchangeably throughout this paper.

The test duct had a rectangular cross-section and the baffle blockages were installed on the upper and lower walls of the duct in a staggered manner. In this orientation, each baffle from one wall was situated in the cross-sectional plane which passes through the midpoint of the baffles on the opposite wall. The staggered arrangement thus obtained provided a zigzag path for the core flow and created the recirculating zones near the walls of the duct and between the neighbouring baffles.

With regard to the boundary conditions, it should be mentioned that the upper and lower walls of the duct were covered with solid naphthalene and were kept at uniform temperature. Therefore, the mass transfer model considered here is analogous to a heat transfer problem in which the walls are ideally isothermal. However, the surface of the baffles was not covered with naphthalene, and the two components that contribute to the heat transfer enhancement simultaneously, i.e. additional surface area and improved mixing (due to altered flow field), were intentionally separated and only the latter component was considered in this study. Transfer characteristics of the wall-attached baffles can be found in ref. [7].

The present investigation was carried out experimentally using air as the working fluid. The study was focused on two regions of the duct, namely, the entrance region, where the velocity and temperature (mass concentration) profiles were simultaneously developing, and the periodic fully developed region far away from the inlet of the duct. The important parameters of the problem were Reynolds number *Re*

NOMENCLATURE

A	cross-sectional area of the duct, WH
A_i	mass transfer area per module, WL
A_t	area of the orifice
C_D	coefficient of discharge of the orifice
$\bar{C}_D$	arithmetic mean of C_D
D	diffusion coefficient
D_h	hydraulic diameter of the duct
f	friction factor
H	vertical spacing between the walls of the duct
h	height of the baffle blockage (Fig. 2)
K	loss coefficient
K_i	mass transfer coefficient for module i
L	width of each module along the duct
M_i	per-module rate of mass sublimation
P	air pressure; perimeter of the duct, $2(H+W)$
P_{nw}	naphthalene vapour pressure at the wall
ΔP	pressure difference across the orifice plate
Q	volumetric flow rate of water (equation (1))
Q_i	volumetric air flow rate at the axial location of module i
R	gas constant for naphthalene vapour
Re	Reynolds number (equation (11))
Re^*	modified Reynolds number
Re_s	Reynolds number of the smooth duct
Sc	Schmidt number
Sh	Sherwood number
Sh_{fd}	periodic fully developed Sherwood number
$Sh_{fd,s}$	periodic fully developed Sherwood number for the smooth duct (at the same pumping power)
Sh_i	Sherwood number for module i
T	temperature
u_{Re}	relative uncertainty of Re
u_{Sh}	relative uncertainty of Sh
u_f	relative uncertainty of f
V	mean fluid velocity
W	duct width (Fig. 2)
X	axial coordinate.

Greek symbols

β	ratio of orifice diameter to pipe diameter
ν	kinematic viscosity
ρ	density
$\rho_{nb,i}$	naphthalene vapour density in bulk at module i
ρ_{nw}	naphthalene vapour density at wall
$\Delta\rho_{n,i}$	wall-to-bulk difference in naphthalene vapour density for module i
σ_n	standard deviation
Φ^*	correction function for Re.

and the height of the baffle blockage h. The Reynolds number (based on the mean fluid velocity and the hydraulic diameter of the duct) ranged from 3000 to 50 000, with the latter parameter (normalized by the height of the duct $H = 1.5$ cm) equal to $h/H = 0$, 0.125, 0.25, and 0.50.

EXPERIMENTAL APPARATUS AND PROCEDURE

The schematic view of the experimental apparatus is shown in Fig. 1. The main components of the apparatus are the test section, the orifice plate, the flow control valve, and the centrifugal fan. The fan operated in the suction mode to draw the laboratory air into the test section of the apparatus, where mass transfer between air and the naphthalene-coated walls of the duct occurred, and to discharge the naphthalene-laden exhaust air to the outdoors. This flow circuit ensured that the laboratory remained free from naphthalene vapor and that the heat generated by the fan would not alter the constancy of the inlet air temperature during an experimental run.

The test section had a modular design, and a typical assembly of modules which forms a portion of the wall of the test section is shown in Fig. 2. In this figure,

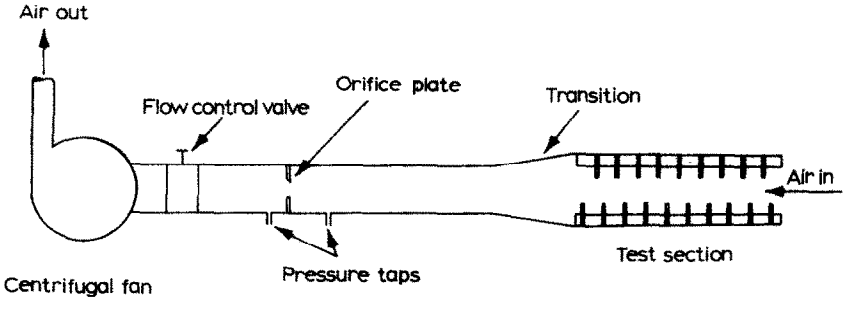

FIG. 1. The experimental apparatus.

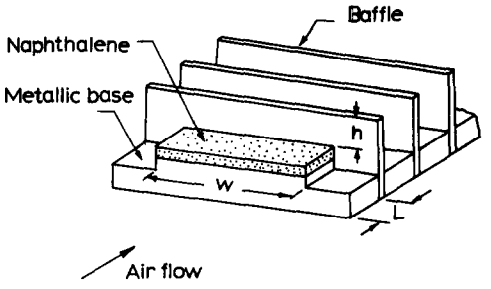

FIG. 2. Perspective view of the assembled modules.

only four modules are shown for simplicity. As seen, each module consists of a metallic base (made of aluminium) and a layer of solid naphthalene coating (3 mm thick). The metallic base was fabricated by machining while the naphthalene coating was accomplished through a casting process. The dimensions of each cast module were $W = 6.0$ cm (the width of the duct) and $L = 1.5$ cm.

The baffles were fabricated from 0.75 mm galvanized sheet metal. Each baffle was placed between a pair of adjacent modules and formed the internal blockages of the test section duct. As mentioned earlier, three different baffle sizes were employed, namely, $h/H = 0.125$, 0.25, and 0.50. These corresponded respectively to 12.5, 25, and 50% blockage of the cross-sectional area.

As many as 40 naphthalene-coated modules were assembled to form the upper and lower walls of the test section. To eliminate the extraneous hydrodynamic disturbances that could be present due to a sudden change of geometry at the downstream end of the duct, 30 additional modules were added to the duct, but these were entirely made of aluminium and did not participate in the mass transfer process. Moreover, the recessed ends of the modules seen in Fig. 2 and the protruded ends of the baffles were covered by a rectangular metallic bar (not shown in the figure) which formed the side walls of the duct. The entire assembly of modules and baffles was then placed in a support housing with rubber gaskets used to seal the joints against leaks.

Before performing the mass transfer experiments, the orifice plate was calibrated. To facilitate the calibration, a separate flow circuit was arranged so that water could flow through the orifice. By measuring the pressure drop ΔP across the orifice and determining the volumetric flow rate of water Q by weighing the water that has passed through the orifice during a certain time interval, the coefficient of discharge of the orifice C_D was calculated from

$$Q = C_D A_t \left(\frac{2\Delta P}{\rho(1-\beta^4)} \right)^{0.5}. \quad (1)$$

where A_t is the area of the orifice (the diameter of the orifice is equal to 2.8 cm), ρ the water density, and β (the ratio of the orifice diameter to the pipe diameter) is equal to 0.7.

The calibration experiment was repeated 72 times for different Reynolds numbers and the corresponding coefficients are shown in Fig. 3. As seen, a certain degree of scatter is observed among the data points. Since we were going to use these results to determine the air flow rate in the mass transfer experiments, it was essential to evaluate the data from the point of view of uncertainty analysis.

To determine the uncertainty interval for C_D, it should be noted that the pressure drop across the orifice was measured by a manometer to within ± 1 mm H_2O, the water was weighed to within ± 0.050 kg, the corresponding flow time was recorded to within ± 0.5 s, and the orifice plate was fabricated from brass by machining to within ± 0.0254 mm. Then, using the method described by Kline [8], and Abernethy *et al.* [9] (and also summarized by Fox and McDonald [10], Appendix E, pp. 716–723), the relative uncertainty in C_D was found to be $\pm 3.4\%$ (odds of 20 to 1). Also, the standard deviation of the coefficients reported in Fig. 3 was determined to be $\sigma_n = 0.01129$, giving $2\sigma_n = 0.0226$ or an uncertainty of $\pm 3.78\%$. With this information, the following value was adopted as the orifice coefficient:

$$C_D = \bar{C}_D \pm 2\sigma_n = 0.5976 \pm 0.0226. \quad (2)$$

Next, the mass transfer experiments were initiated. During each data run, the air temperature was recorded several times by a mercury thermometer with a resolution of 0.25°C. The naphthalene vapour pressure and other properties were then evaluated at the arithmetic mean of the recorded temperatures. To determine the rate of mass sublimation at each axial station along the duct, the modules were individually weighed on a Sartorius balance before and after each data run, and the mass changes were determined to within 0.1 mg. Mass changes were typically around 15 mg.

The mass transfer experiments were complemented by measurements of the pressure drop. The pressure measurement experiments were performed on the same test section while the metallic modules were coated with a 3 mm layer of solid paraffin (instead of naphthalene), to prevent the height of the duct from changing due to sublimation. A total of 21 pressure taps were mounted on the side wall of the test section. The pressure signals were conveyed through plastic tubing to a water manometer, and the pressures recorded.

DATA REDUCTION

The mass transfer coefficient for a typical module i was evaluated from its conventional defining equation

$$K_i = M_i / A_i \Delta \rho_{n,i} \quad (3)$$

where M_i is the rate of mass sublimation from the module, determined from the amount of mass sublimated from module i during the run time, A_i the mass transfer surface area ($A_i = WL = 6.0 \times 1.5\,\text{cm}^2$),

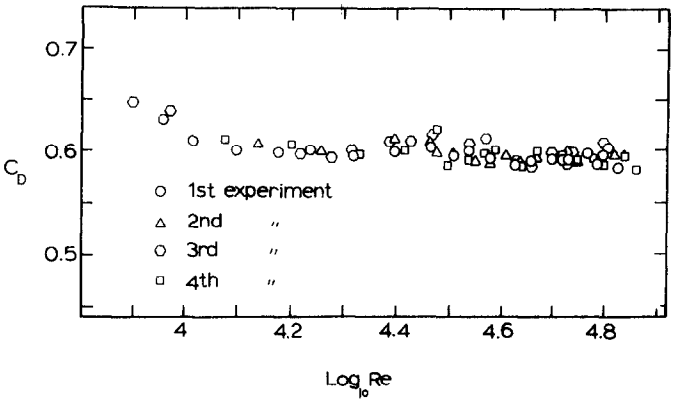

FIG. 3. Coefficient of discharge of the orifice plate.

and $\Delta\rho_{n,i}$ the wall-to-bulk difference in naphthalene vapour density at the axial midpoint of the module

$$\Delta\rho_{n,i} = \rho_{nw} - \rho_{nb,i}. \tag{4}$$

The evaluation of $\Delta\rho_n$ requires knowledge of the axial variation of the bulk vapour density of naphthalene in the air stream ρ_{nb} and the naphthalene vapour density at the wall ρ_{nw}. To determine ρ_{nw}, the naphthalene vapour pressure at the wall was evaluated from Sogin's vapour pressure–temperature correlation [11]

$$\log_{10} P_{nw} = 13.564 - \frac{3729.4}{T} \tag{5}$$

and then substituted into the ideal gas equation

$$\rho_{nw} = \frac{P_{nw}}{RT}. \tag{6}$$

In equation (5), the temperature T is in kelvin and the vapour pressure P_{nw} is in pascal. It should be noted that the test section was isothermal and that ρ_{nw} was the same for all modules.

To find ρ_{nb} at the axial midpoint of a module, the following expressions were developed from a mass balance performed on a control volume that encompassed the portion of the duct from the inlet up to the axial midpoint of the ith module ($i \geqslant 3$)

$$\rho_{nb,i} = \left(1.5M_1 + 2\sum_{j=2}^{i-1} M_j + 1.5M_i\right) \Big/ Q_i. \tag{7}$$

The first and second modules were treated as special cases and, in a similar manner, the following expressions were obtained for them:

$$\rho_{nb,1} = M_1/Q_1 \tag{8}$$

$$\rho_{nb,2} = 1.5(M_1 + M_2)/Q_2. \tag{9}$$

It should be noted that the coefficient of 1.5 for M_1 appeared when the rates of mass sublimation of the first two modules on the lower wall were approximated by those of the opposite modules on the upper wall of the duct.

In equations (7)–(9), M_i and Q_i represent, respectively, the rate of mass sublimation and the volumetric air flow rate corresponding to module i. It should be mentioned that the pressure drop along the duct was relatively large, and the volumetric air flow rate Q_i was evaluated at the local pressure.

Also, it is noteworthy that the sublimation of naphthalene increases the height of the duct cross-section from $H = 1.5$ cm to a larger value, thus increasing the hydraulic diameter of the duct D_h during the experiment. In order to minimize these changes, the duration of each data run was adjusted in such a way that the naphthalene sublimation did not lower the surface of solid naphthalene by more than 0.0254 mm. Knowing that the original value of the hydraulic diameter D_h ($D_h = 4A/P$, $A = WH$, $P = 2(W+H)$) of the duct was 2.4 cm, this amount of sublimation increased D_h by a negligible 0.27%. Nevertheless, even these small changes were taken into account.

Finally, the mass transfer coefficients evaluated from equation (3) were normalized through the definition of Sherwood number and presented for the ith module as

$$Sh_i = K_i D_h/D \tag{10}$$

where D is the diffusion coefficient. This coefficient was determined from the definition of Schmidt number $Sc = \nu/D$. For naphthalene diffusion in air, $Sc = 2.5$ [11]. Due to small concentrations of naphthalene vapour (typically about 2.18×10^{-5} kg m^{-3} at the end of the test section), the kinematic viscosity ν was taken as that for pure air.

The mass (heat) transfer results will be presented in terms of the duct Reynolds number Re, defined as

$$Re = VD_h/\nu \tag{11}$$

where V is the mean fluid velocity across the flow area $A = WH$.

In the next section, we shall present the mass (heat) transfer results; but before that, a few words are worthy of mention regarding the uncertainty of the results.

The barometric pressure which was needed for evaluation of the absolute pressures was recorded to

within ± 0.01 cm Hg. The uncertainty in the readings of the manometer, thermometer, dimensions of the duct, duration time of the runs, and mass of the modules were, respectively, equal to ± 1 mm H_2O, ± 0.25°C, ± 0.0254 mm, ± 1 s, and ± 0.1 mg. From the analysis of the propagation of these values into the final results, we obtained the following relative uncertainties:

$$u_{Re} = \pm 3.5\% \quad \text{(odds of 20 to 1)}$$

$$u_{Sh} = \pm 3.37\% \quad \text{(odds of 20 to 1)}$$

$$u_f = \pm 7.8\% \quad \text{(odds of 20 to 1)}.$$

In these expressions, the quantities u_{Re}, u_{Sh}, and u_f denote the relative uncertainty of the Reynolds number, the Sherwood number, and the friction factor (to be defined later), respectively.

PRESENTATION OF THE MASS (HEAT) TRANSFER RESULTS

As a first step, the transfer characteristics of the smooth duct (with no internal baffle blockage) was investigated. The fully developed results are shown in Fig. 4 (open circles). Also shown in this figure are the well-known Petukhov–Popov correlation [12] and Gnielinski's modified version [13]. Knowing that these correlations were obtained theoretically and compared with many experimental heat transfer results, the close agreement seen in this figure supports the present experimental approach.

Next, attention is turned to the periodic fully developed Sherwood number Sh_{fd} for the duct with repeated-baffle blockages. It is seen that as soon as the smallest blockage is introduced into the duct (i.e. 12.5% corresponding to $h/H = 0.125$), the Sherwood number is increased. The reason is that in turbulent flow, a large portion of the thermal (mass transfer) resistance lies in the laminar sublayer (wall layer), and the introduction of any solid protuberance at the wall would disturb and break this layer, resulting in higher transfer coefficients. As the extent of blockage is increased, not only the laminar sublayer may be completely removed, but also a recirculating zone appears behind the baffles which has an additional enhancing effect on the transfer coefficients. The presence of these recirculating zones has been shown by Berner *et al.* [4] and Kelkar and Patankar [14]. They have also shown that at higher Reynolds number, the size of the recirculating zones is affected and that vortices are shed from the tip of the baffles. All these activities tend to increase the turbulence in the air stream and thus increase the heat (mass) transfer coefficients.

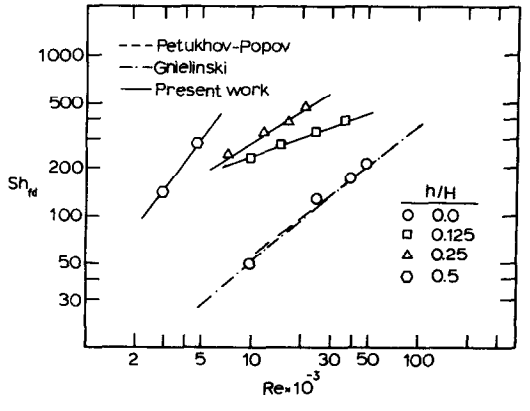

FIG. 4. Fully developed Sherwood numbers.

The solid lines passing through the data points of Fig. 4 are the least-squares fits. The equations of these lines are

$$Sh_{fd} = 5.89Re^{0.398} \quad (h/H = 0.125) \qquad (12)$$

$$= 1.11Re^{0.605} \quad (h/H = 0.25) \qquad (13)$$

$$= 6.94Re^{1.520} \quad (h/H = 0.50). \qquad (14)$$

Equations (12)–(14) indicate that as the height of the baffle is increased, Sh_{fd} has a stronger dependence on Reynolds number. By adopting a recirculating zone and vortex shedding point of view for the flow field, we postulate that the increased dependence of Sh_{fd} on Re is due to smaller but stronger recirculating zones and more frequent vortex shedding as the h/H values are increased.

Attention is now turned to Fig. 5 where Sherwood numbers are plotted in the entrance region of the smooth duct. In this figure, the ordinate is the normalized Sherwood number Sh/Sh_{fd} and the abscissa is the axial distance from the inlet of the duct (with $X = 0$ corresponding to the inlet) nondimensionalized by the hydraulic diameter D_h. In addition, the Reynolds number appears as a parameter.

An overall examination of the figure reveals a familiar trend, namely, large transfer coefficients near the inlet followed by a rapid decrease in coefficients and, finally, approaching the fully developed values. The relatively large initial values of Sh/Sh_{fd} are due to large mass concentrations near the inlet, while the growth of the boundary layer and the resulting decrease in gradients are responsible for the subsequent lower values of Sh/Sh_{fd}.

It is well known that heat (mass) transfer coefficients at the entrance region are strongly dependent on the duct inlet geometry [15]. In this connection, it should be mentioned that the test section employed in the present investigation has a 90° sharp-edged (abrupt contraction) inlet. As fluid enters the duct, it cannot follow the sharp profile of the inlet, and flow separation occurs. This phenomenon has a pronounced effect on heat (mass) transfer. The solid line in Fig. 5 has been plotted for heat transfer in isothermal tubes with a sharp-edged inlet using air at $Re = 50\,000$ [15]. The effect of flow separation, recirculation, and reattachment appears in the form of the dome-shaped portion of this curve near the inlet.

The same phenomenon also exists near the entrance of a sharp-edged inlet of the rectangular duct. However, the point of reattachment, as shown by

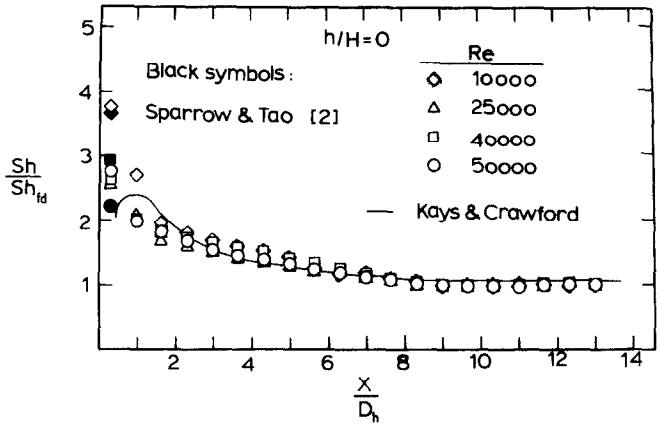

FIG. 5. Sherwood numbers in the entrance region of the smooth duct ($h/H = 0$).

Sparrow and Tao [2] is very close to the inlet (about $X/D_h = 0.42$) and, in the present study, occurs on the first module of the test section (the axial length of the module is $L/D_h = 0.625$). In fact, the data reported in Fig. 5 are the average values of Sh/Sh_{fd} over the axial distance of $0.625D_h$.

It is seen that except for the first few data points, the Reynolds number has a negligible effect on Sh/Sh_{fd}. Indeed, the values of Sh and Sh_{fd} both depend strongly on Reynolds number, but the ratio of these quantities has a different behaviour.

The first set of data points of the present investigation has been compared with that of Sparrow and Tao [2] in Fig. 5. The black diamond, triangle, square, and circle correspond, respectively, to $Re = 10\,920$, 21 670, 32 600, and 45 470. Examination of both sets of data reveal that the effect of Re on Sh/Sh_{fd} is not in a particular direction. This irregularity of behaviour may be attributed to the inherently unstable (and perhaps unpredictable) character of the flow separation zone. However, considering the many differences between the two studies such as different aspect ratios and Reynolds numbers, the agreement between the two sets of data is well within the experimental uncertainty.

The effect of the baffle blockages on the transfer characteristics of the entrance region of the duct for $h/H = 0.125$, 0.25, and 0.50, is shown in Fig. 6. The ordinate Sh/Sh_{fd} is the Sherwood number that has been normalized by the periodic fully developed Sherwood number at the same h/H.

The general behaviour of these curves is similar and reminiscent of that of the entrance region of a smooth duct. Beginning with a slightly larger value, Sh/Sh_{fd} decreases and approaches the fully developed value. The first set of data points in Fig. 8 is an exception to this rule. In fact, it should be noted that the same mechanism that is responsible for large heat (mass) transfer coefficients near the inlet of the duct (Fig. 5), i.e. flow separation and recirculation, is now present everywhere throughout the duct. Therefore, the magnitude of Sh_{fd} seen in the ordinate Sh/Sh_{fd} is comparable to the values of Sh in the separated flow region near the inlet. At $h/H = 0.5$, it appears that the recirculating zones created by the baffles are stronger than those at the inlet, and as a result the first set of points has a lower Sh/Sh_{fd}.

A quantity of practical importance in design of compact heat exchange devices is the entrance length L_e of the duct. By adopting the 5%-of-Sh_{fd} criterion for the entrance length (i.e. $Sh/Sh_{fd} = 1.05$), the values of L_e were determined for $h/H = 0$, 0.125, 0.25, and 0.50, and the results are shown in Table 1. As the extent of blockage is increased, the resulting higher turbulence and improved mixing decrease the entrance length.

FRICTION FACTOR

The pressure measurement data were employed to evaluate the friction factor in the periodic fully developed region from

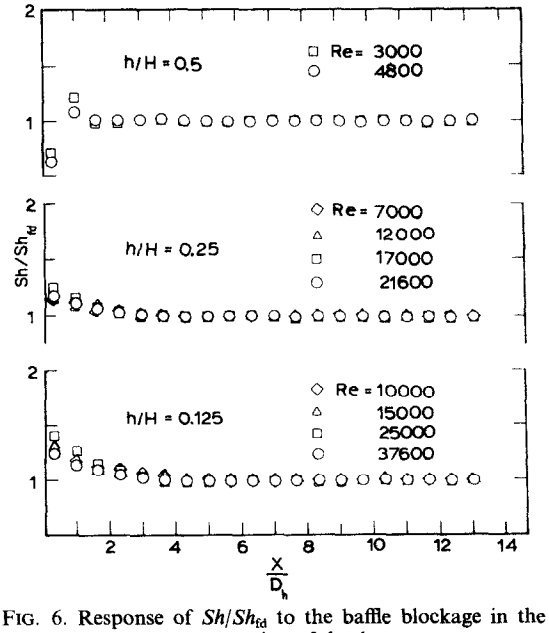

FIG. 6. Response of Sh/Sh_{fd} to the baffle blockage in the entrance region of the duct.

Table 1. Variation of thermal (mass concentration) entrance length with h/H

h/H	L_e/D_h
0	7.93
0.125	2.86
0.25	2.09
0.50	1.39

$$f = (-\mathrm{d}P/\mathrm{d}X)D_h/\tfrac{1}{2}\rho V^2 \quad (15)$$

and are plotted in Fig. 7. The friction factors for the smooth duct are compared with the Blasius equation in the lower part of the figure. In order to have a meaningful comparison, the Blasius equation has been modified for the present problem according to the recommendation of Jones [16], and the dashed line in Fig. 7 is expressed by

$$f = 0.3164 Re^{*-0.25} \quad (16)$$

where the modified Reynolds number

$$Re^* = \Phi^*\left(\frac{H}{W}\right)Re \quad (17)$$

and the function $\Phi^*(H/W) = 0.867$ for the rectangular duct of this investigation. The maximum difference between the data points and the values of f predicted by the modified Blasius equation is 4.7%, and is well within the estimated relative uncertainty $u_f = \pm 7.8\%$.

The effect of h/H on f is shown in the upper part of the figure. As the extent of the blockage increases, the friction factor increases too. Using the least-squares method, the experimental data are correlated by the power law $f = a\ Re^{-b}$, where $(a, b) = (2.02, 0.165)$, $(106.46, 0.440)$, and $(4.46 \times 10^4, 0.84)$, respectively, for $h/H = 0.125$, 0.25, and 0.50.

Examination of these correlations indicates that as h/H is increased, the dependence of f on Re at first decreases, but at higher values of h/H a stronger dependence on Re is observed. It appears that the pressure losses are governed by two components of drag, namely, viscous and form drag, and the relative importance of each component determines the trend of the f distribution. At $h/H = 0.125$, seemingly the latter component is more important than the former. But as h/H is increased to 0.25 and then to 0.50, we suggest that because of the enhanced strength of the recirculating zones, the velocity gradients increase and the viscous drag becomes more important.

The pressure drop in pipe fittings is often given in terms of a loss coefficient K defined as $K = \Delta P/\frac{1}{2}\rho V^2$. The values of K for $h/H = 0.125$, 0.25, and 0.50 are given in the figure.

EVALUATION OF PERFORMANCE

To examine the thermal hydraulic performance of the duct and to determine the optimum value of h/H, we have combined the friction factor and heat (mass) transfer results in Fig. 8. Here the ordinate $Sh_{fd}/Sh_{fd,s}$ is the ratio of Sherwood number for the duct with baffle blockage to the Sherwood number of a smooth duct with the same pumping power requirement. The abscissa is the Reynolds number of the smooth duct Re_s. It can be shown that under equal pumping power, the data of the two ducts are related through

$$(f\,Re^3)_{\text{with blockage}} = (f\,Re^3)_{\text{smooth}}.$$

Clearly, the optimum h/H depends on the Reynolds number. In the range of Reynolds numbers considered in this work, as Re_s increases, the performance corresponding to $h/H = 0.5$ improves, while that corresponding to other values of h/H degenerates. It

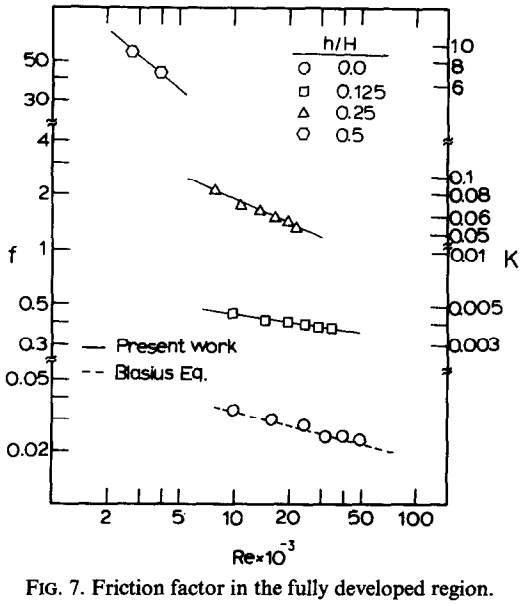

FIG. 7. Friction factor in the fully developed region.

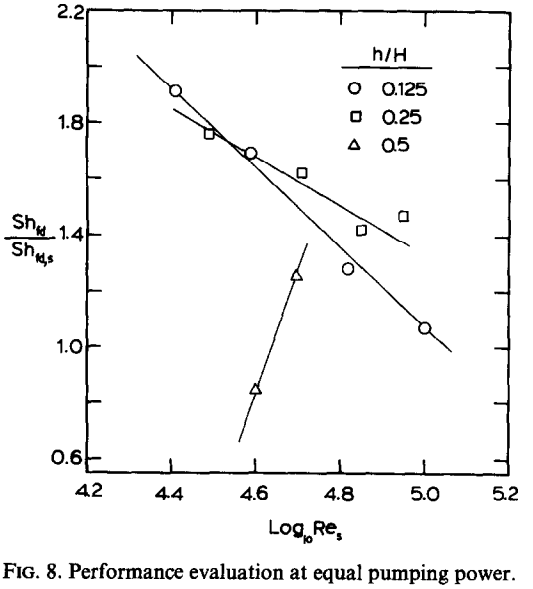

FIG. 8. Performance evaluation at equal pumping power.

appears that at lower Reynolds numbers, the smaller values of h/H yield a better performance. In this case, the mass (heat) transfer coefficient increases by as much as 90% of that of the smooth duct with the same pumping power.

CONCLUDING REMARKS

The present experimental work has revealed the mass (heat) transfer and pressure drop characteristics of rectangular ducts with staggered baffle blockages. The experiments were carried out by a mass transfer technique and for a boundary condition which is equivalent to uniform wall temperature in the analogous heat transfer problem.

The transfer characteristics of the duct were examined in the periodic fully developed and the entrance region, and the distribution of Sherwood numbers revealed large enhancements due to the presence of baffle blockages. Further, it was shown that the baffles affected the entrance length of the duct, and the entrance length decreased monotonically with an increase in the height of the baffles.

The pressure drops were also investigated, and it was found that the baffles increase the pressure drop much faster than they increase the mass (heat) transfer coefficients. Finally, the mass transfer and pressure data were combined under the equal pumping power condition, and enhancements of up to 90% occurred for the smallest baffle.

REFERENCES

1. J. C. Han, L. R. Glicksman and W. M. Rohsenow, An investigation of heat transfer and friction for rib-roughened surfaces, *Int. J. Heat Mass Transfer* **21**, 1143–1156 (1978).
2. E. M. Sparrow and W. Q. Tao, Enhanced heat transfer in a flat rectangular duct with streamwise-periodic disturbances at one principal wall, *ASME J. Heat Transfer* **105**, 851–861 (1983).
3. M. Molki and C. M. Yuen, Effect of interwall spacing on heat transfer and pressure drop in a corrugated-wall duct, *Int. J. Heat Mass Transfer* **29**, 987–997 (1986).
4. C. Berner, F. Durst and D. M. McEligot, Flow around baffles, ASME Paper 83-WA/HT-9 (1983).
5. J. C. Han, J. S. Park and C. K. Lei, Heat transfer enhancement in channels with turbulence promoters, ASME Paper 84-WA/HT-72 (1984).
6. E. R. G. Eckert, Analogies to heat transfer processes. In *Measurements in Heat Transfer* (Edited by E. R. G. Eckert and R. J. Goldstein), pp. 397–423. Hemisphere, Washington, DC (1976).
7. E. M. Sparrow and K. P. Wachtler, Transfer coefficients on the surfaces of a transverse plate situated in a duct flow, *Int. J. Heat Mass Transfer* **21**, 761–767 (1978).
8. S. J. Kline, The purposes of uncertainty analysis, *ASME J. Fluids Engng* **107**, 153–160 (1985).
9. R. B. Abernethy, R. P. Benedict and R. B. Dowdell, ASME measurement uncertainty, *ASME J. Fluids Engng* **107**, 161–164 (1985).
10. R. W. Fox and A. T. McDonald, *Introduction to Fluid Mechanics* (3rd Edn), pp. 716–723. Wiley, New York (1985).
11. H. H. Sogin, Sublimation from disks to air streams flowing normal to their surfaces, *Trans. Am. Soc. Mech. Engrs* **89**, 61–69 (1958).
12. B. V. Karlekar and R. M. Desmond, *Heat Transfer* (2nd Edn), p. 497. West, St. Paul, Minnesota (1982).
13. V. Gnielinski, New equations for heat and mass transfer in turbulent pipe and channel flow, *Int. Chem. Engng* **16**, 359–386 (1976).
14. K. M. Kelkar and S. V. Patankar, Numerical prediction of flow and heat transfer in a parallel plate channel with staggered fins, *ASME J. Heat Transfer* **109**, 25–30 (1987).
15. W. M. Kays and M. E. Crawford, *Convective Heat and Mass Transfer* (2nd Edn). McGraw-Hill, New York (1980).
16. O. C. Jones, Jr., An improvement in the calculation of turbulent friction in rectangular ducts, *J. Fluids Engng* 173–180 (1976).

TRANSFERT THERMIQUE TURBULENT DANS DES CANAUX RECTANGULAIRES AVEC DES BLOCAGES PAR BAFFLES

Résumé—On étudie expérimentalement le transfert de chaleur et la perte de pression dans un canal rectangulaire avec des blocages successifs par des déflecteurs. Ceux-ci sont arrangés d'une façon étagée avec espacement axial fixe. Les coefficients de transfert sont évalués dans la région établie périodique et à l'entrée du canal. La présence des baffles augmente ces coefficients. La longueur d'entrée du canal est sensiblement réduite par les baffles. Les données de perte de pression et de transfert de chaleur sont utilisées pour évaluer la performance du canal.

WÄRMEÜBERTRAGUNG BEI TURBULENTER STRÖMUNG IN RECHTECKKANÄLEN MIT EINGEBAUTEN UMLENKBLECHEN

Zusammenfassung—Es wurde eine experimentelle Untersuchung durchgeführt, um Wärmeübertragung und Druckverlust in rechteckigen Kanälen mit hintereinanderliegenden Umlenkblechen zu bestimmen. Die Umlenkbleche sind bei konstantem axialem Abstand versetzt angeordnet. Die Wärmeübergangs-Koeffizienten sind für den Einlaufbereich des Kanals und für das Gebiet der periodisch voll entwickelten Strömung bestimmt. Die Umlenkbleche führen zur Erhöhung der Wärmeübergangs-Koeffizienten. Die Länge des Einlaufbereiches wird durch die Umlenkbleche wesentlich verkürzt. Schließlich werden die Daten über Druckverluste und Wärmeübergangs-Koeffizienten dazu benutzt, die thermische Leistung des Kanals zu bestimmen.

ТУРБУЛЕНТНЫЙ ТЕПЛОПЕРЕНОС В КАНАЛАХ ПРЯМОУГОЛЬНОГО СЕЧЕНИЯ С БЛОЧНЫМИ ПЕРЕГОРОДКАМИ

Аннотация—Экспериментально исследуется теплоперенос и перепад давления в канале прямоугольного сечения с блочными перегородками. Перегородки расположены в шахматном порядке с фиксированным интервалом по оси. Оцениваются коэффициенты теплопереноса в периодической полностью развитой, а также во входной областях канала. Наличие перегородок приводит к увеличению этих коэффициентов. Длина входного участка значительно уменьшается за счет перегородок. Данные по перепаду давления и теплопереносу используются для оценки тепловых характеристик канала.